Supporting Information

A "Simple" Donor-Acceptor AIEgen with Multi-Stimuli Responsive Behavior

Jing Zhang,‡[a] Aisen Li,‡[b] Hang Zou,‡[a] Junhui Peng,[a] Jiali Guo,[c] Wenjie Wu,[a] Haoke Zhang,[a] Jun Zhang,[a] Xinggui Gu,[d] Weiqing Xu,*[b] Shuping Xu,[b] Sheng Hua Liu,[e] Anjun Qin,[c] Jacky W. Y. Lam[a] and Ben Zhong Tang*[ac]

[a] Department of Chemistry, Hong Kong Branch of Chinese National Engineering Research Center for Tissue Restoration and Reconstruction, Institute for Advanced Study, Department of Chemical and Biological Engineering, Institute of Molecular Functional Materials, Division of Life Science and State Key Laboratory of Molecular Neuroscience, The Hong Kong University of Science and Technology (HKUST), Clear Water Bay, Kowloon, Hong Kong, China. E-mail: tangbenz@ust.hk

[b] State Key Laboratory of Supramolecular Structure and Materials, College of Chemistry, Jilin University, Changchun 130012, P. R. China. E-mail: xuwq@jlu.edu.cn

[c] Center for Aggregation-Induced Emission, SCUT-HKUST Joint Research Institute, State Key Laboratory of Luminescent Materials and Devices, South China University of Technology, Guangzhou 510640, China.

[d] Beijing Advanced Innovation Center for Soft Matter Science and Engineering, Beijing University of Chemical Technology, Beijing 100029, China.

[e] Key Laboratory of Pesticide and Chemical Biology, Ministry of Education, College of Chemistry, Central China Normal University, Wuhan 430079, China.

‡ These two authors contributed equally to this work.

Materials and Methods

^{1}H and ^{13}C NMR spectra were measured on a Bruker AVIII 400 MHz NMR spectrometer using deuterated chloroform as solvent and tetramethylsilane (TMS; $\delta = 0$) as an internal reference. High-resolution mass spectra (HRMS) were recorded on a GCT Premier CAB 048 mass spectrometer system operating in a MALDI-TOF mode. UV spectra were measured on a Varian CARY 50 UV-visible spectrophotometer. PL spectra were recorded on a PerkinElmer LS 55 spectrofluorometer. The high-pressure experiments were carried out in diamond anvil cell (BGI-type DAC) with 500 μm in diameter. T301 stainless steel sheet was drilled a hole with 200 μm in diameter to serve as gasket. A small ruby chip in the sample chamber was used for in situ pressure calibration based on the fluorescence of the ruby R1 line. Silicone oil was used as a pressure-transmitting medium (PTM) to obtain the hydrostatic pressure. The measurements of the ruby chip were performed at a Horiba Jobin Yvon T64000 Raman spectrometer with a 1800 gr/mm holographic grating with a laser of 532 nm. The high-pressure PL spectra under hydrostatic pressure were measured using a fluorescence microscope (IX71, Olympus 20 ×, numerical aperture = 0.4) equipped with a spectrometer (Horiba Jobin Yvon iHR320), and the light source of which was a mercury lamp with an excitation wavelength of 365 nm. The high-pressure Raman spectra were recorded by using a confocal Raman system (LabRAM Aramis, Horiba Jobin Yvon) and the excitation source was a 785 nm laser with power of 23 mW for Raman.[1-3] Electrochemical measurements were performed with a CHI 660C potentiostat (CHI, Austin, TX, USA). A solution of the studied compound and supporting electrolyte in dry CH_2Cl_2 was placed in a three-electrode single-compartment cell. The solution was deaerated by argon bubbling on a frit for about 10 min before the measurement. The analyte (target compound, intermediate) and electrolyte (n-Bu_4NPF_6) concentrations were typically 10^{-3} and 10^{-1} mol dm^{-3}, respectively. A 500-μm diameter platinum disk working electrode, a platinum wire counter electrode, and an Ag/Ag^{+} reference electrode were used. Spectroelectrochemical UV/Vis/NIR experiments at room temperature were performed with an airtight optically transparent thin-layer electrochemical (OTTLE) cell (optical pathlength of ca. 200 μm) equipped with a Pt minigrid working electrode and CaF_2 windows.[4] The cell was positioned in the sample compartment of a Shimadzu UV-3600 UV/Vis/NIR spectrophotometer. Spectroelectrochemical fluorescence measurements were performed using a spectroelectrochemical quartz cell (pathlength of 1.0 mm) with a three-electrode system comprising a light-transparent platinum gauze (100 mesh, 7.0 × 5.0 mm) as the working electrode, a platinum wire as the counter electrode, and an Ag wire as the reference electrode. *In situ* spectroelectrochemical studies all were carried out by increasing the anodic potential in steps of 10 or 20 or 30 mV. Controlled-potential electrolyses were carried out with a CHI 660C potentiostat. Sample concentrations were ca. 1×10^{-3} mol dm^{-3}, and dry 10^{-1} mol dm^{-3} n-Bu_4NPF_6 was used as the supporting electrolyte. Absolute fluorescence quantum yields were measured on a Hamamatsu C11347 Absolute PL quantum yield spectrometer. Fluorescence lifetimes were measured on a Hamamatsu C11367 compact fluorescence lifetime spectrometer. XRD studies were conducted on a Shimadzu XRD-6000 diffractometer using Ni-filtered and graphite-monochromated Cu-K_α radiation (λ = 1.54 Å, 40 kV, 30 mA).

Device fabrication and characterization

Multilayer OLEDs were fabricated by the vacuum-deposition method. 95 nm indium tin oxide (ITO) coated glass substrates with a sheet resistance of 15-20 Ω sq^{-1} were subjected to a routine cleaning process of acetone, isopropyl alcohol, detergent, deionized water, and isopropyl alcohol under ultrasonic bath and treated with O_2 plasma for 10 mins. Organic layers and cathode were sequentially deposited on the ITO-coated glass substrates by thermal evaporation under high vacuum (< 5×10^{-4} Pa). And the deposition rates are 1.0 Å s^{-1} for organic layers, 0.1 Å s^{-1} for LiF layer and 3-5 Å s^{-1} for Al cathode, respectively. The active area of each device was 9 mm^2. The electroluminescence spectra (EL), the current density-voltage characteristics (J-V) and the current density-voltage-luminance curves characterizations (J-V-L) of the OLEDs were detected by a Photo Research SpectraScan PR-745 Spectroradiometer and a Keithley 2450 Source Meter and they are

recorded simultaneously. All the device characterizations were carried out at room temperature under ambient laboratory conditions.

Computational Details

The ground state (S0) and excited states geometries (S1) were optimized at DFT-B3LYP/6-31G(d) level. The molecular orbitals of the highest occupied molecular orbital (HOMO) and the lowest unoccupied molecular orbital (LUMO) were generated using GaussView 5.0. Four conformations with different twisting were generated and the twisting dihedral angle, C22-N1-C21-C28, of the conformations were set to 0-90°. The fluorescence spectra of all the eight conformations, including the ground state conformation, were computed with fixed twisting by time-dependent density functional theory (TDDFT) at BLY3P/6-31G(d) level. Fequency calculations on the resulting optimized geometries showed no imaginary frequencies All the theoretical calculations were performed in Gaussian 09 program.

MTT

Cell viabilities were evaluated by MTT assays. Cells were seeded in 96-well plates at a density of about 5000-8000 cells per well and grown for 24 h. Then the medium in each well was replaced with 200 μL fresh DMEM containing various concentrations of compound **1**. After 24 h, the medium in each well was replaced with MTT solution (5 mg/mL). After 4 h, 100 μL DMSO was added into each well to dissolve the formazan, and the absorbances of plates at 570 nm were analyzed with a microplate reader (Perkin-Elmer Victor3TM). Each experiment was performed at least three times.

Cell culture

MCF-7 cells were cultured in DMEM containing 10% FBS and antibiotics (100 units/mL penicillin and 100 μg/mL streptomycin) in a 5% CO_2 humidity incubator at 37 °C and sub-cultured every 2 days. MCF-7 cells are treated with oleinic acid (10 μg/ mL) for 6 h to induce the formation of lipid drops intracellularly.

Two-Photon Fluorescence Imaging in Cells

MCF-7 cells were seeded in a 35 mm Glass Bottom Cell Culture Dish with a density of 1×10^5 cells per well and grew to a desired confluence. After treated with or without oleinic acid, the cell staining was conducted by replacing the cell medium with dye-containing medium. The cells were imaged using a two-photon microscope (Olympus FV1200MPE). Excitation wavelength: 780 nm. The two-photon fluorescence emitted from compound **1** were captured through two filters: 420-460 nm (blue) and 495-540 nm (green). For BODIPY (10 μg/mL, 30 min) and Lysotracker Red (LTR, 100 nM, 30 min), the excitation wavelength was 970 nm and the emission filter were 495−540 nm (BODIPY) and 575-630 nm (LTR).

Tissue Two-Photon Fluorescence Imaging

All experiments conformed to the Guide for the Care and Use of Laboratory Animals published by the US National Institutes of Health (NIH Publication No. 85-23, revised 1996). Male six-week-old nude mouse were purchased from Beijing Vital River Laboratory Animal Technology Co., Ltd and fed on a high-fat diet containing 15% fat and 0.25% cholesterol for 6 months. Mice were anaesthetized and sacrificed; the Mesenteric adipose tissue was carefully isolated, followed by staining with 5 mM compound **1** for 30 min. and the tissue were imaged by a two-photon microscope (Olympus FV1200MPE). Two-photon excitation wavelength: 780 nm. The emission range λ_{em} = 420-460 nm (blue), and λ_{em}=495-540 (green). Using Imaris 8.1 to reconstructed 3D two-photon images(Z-stack).

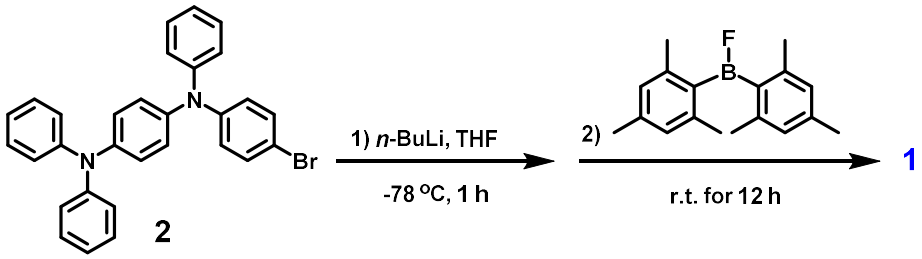

Scheme S1. General synthetic route to compound **1**.

Experimental Section

General materials and synthesis

The general synthetic route to compound **1** is outlined in Scheme S1. All manipulations were carried out under a dry argon atmosphere using standard Schlenk techniques, unless stated otherwise. Solvents were pre-dried and distilled under argon prior to use, except those used directly for spectroscopic measurements, which were of spectroscopic grade. The precursor **2** was prepared according to procedure described in the literature.[5] Other reagents were purchased and used as received.

Synthesis of compound **1**: N^1-(4-bromophenyl)-N^1,N^4,N^4-triphenylbenzene-1,4-diamine (compound **2**) (490 mg, 1.00 mmol) was dissolved in anhydrous THF (30 mL) under nitrogen, and the resulting mixture was cooled to -78 °C. To this solution, *n*-BuLi (0.5 mL, 2.5 M in hexane) was added slowly and the resulting solution was stirred for 1 h at -78 °C. Dimesitylboron fluoride (402 mg, 1.5 mmol) was dissolved in THF (10 mL) and then slowly added to the reaction solution at -78 °C. The mixture was allowed to warm to room temperature with stirring overnight. The solvent was then removed in vacuo, and the residue was purified by chromatography on silica gel (petroleum ether/ dichloromethane 8:1, v/v). The product was precipitated from a solution in CH_2Cl_2 by adding MeOH to give 547 mg (79%) of **1** as a yellow-green powder. ^{1}H NMR ($CDCl_3$, 400 MHz, ppm): δ 7.35 (d, J = 8 Hz, 2H), 7.18-7.31 (m, 8H), 6.98-7.10 (m, 11H), 6.90 (d, J = 8 Hz, 2H), 6.79 (s, 4H), 2.28 (s, 6H), 2.06 (s, 12H); ^{13}C NMR ($CDCl_3$, 100 MHz, ppm): 151.4, 147.7, 146.6, 144.2, 141.9, 141.2, 140.7, 138.7, 137.9, 129.4, 129.2, 129.1, 128.0, 127.1, 125.6, 124.9, 124.1, 124.0, 122.7, 118.9 (Ar); HRMS (MALDI-TOF): *m/z*: $[M]^+$ calcd for $C_{48}H_{45}BN_2^+$: 660.3676; found: 660.3665.

NMR and MS spectra

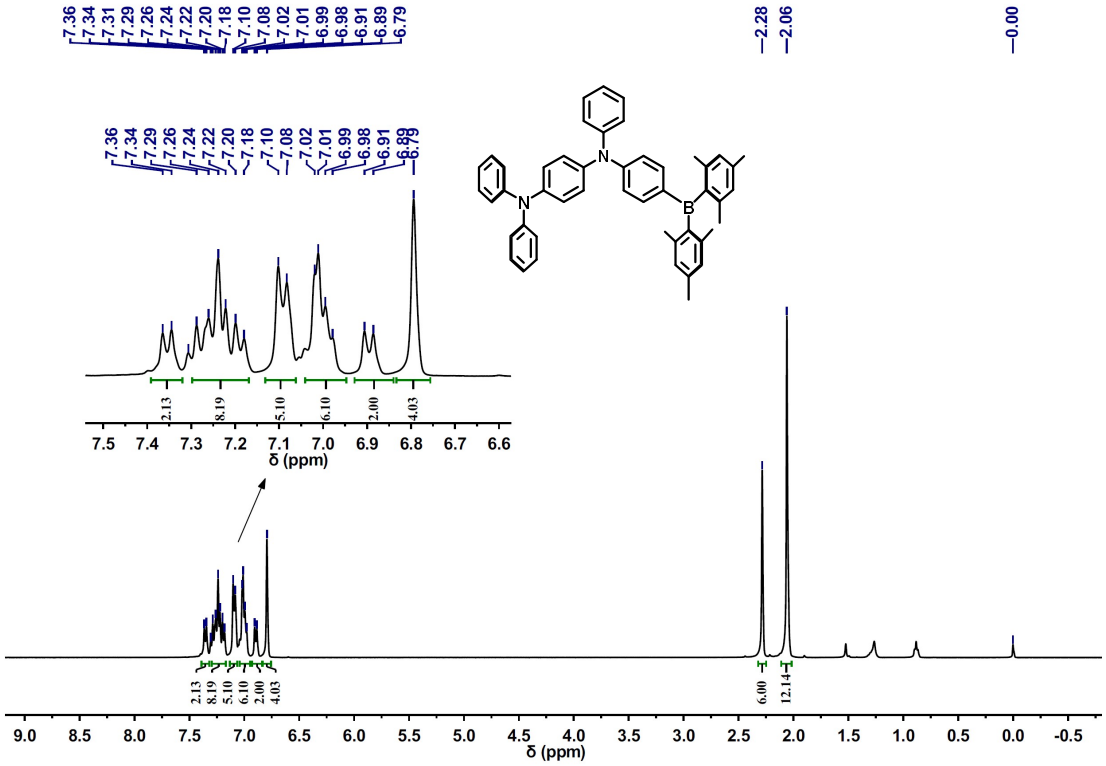

Figure S1. ^{1}H NMR spectrum of **1** in $CDCl_3$.

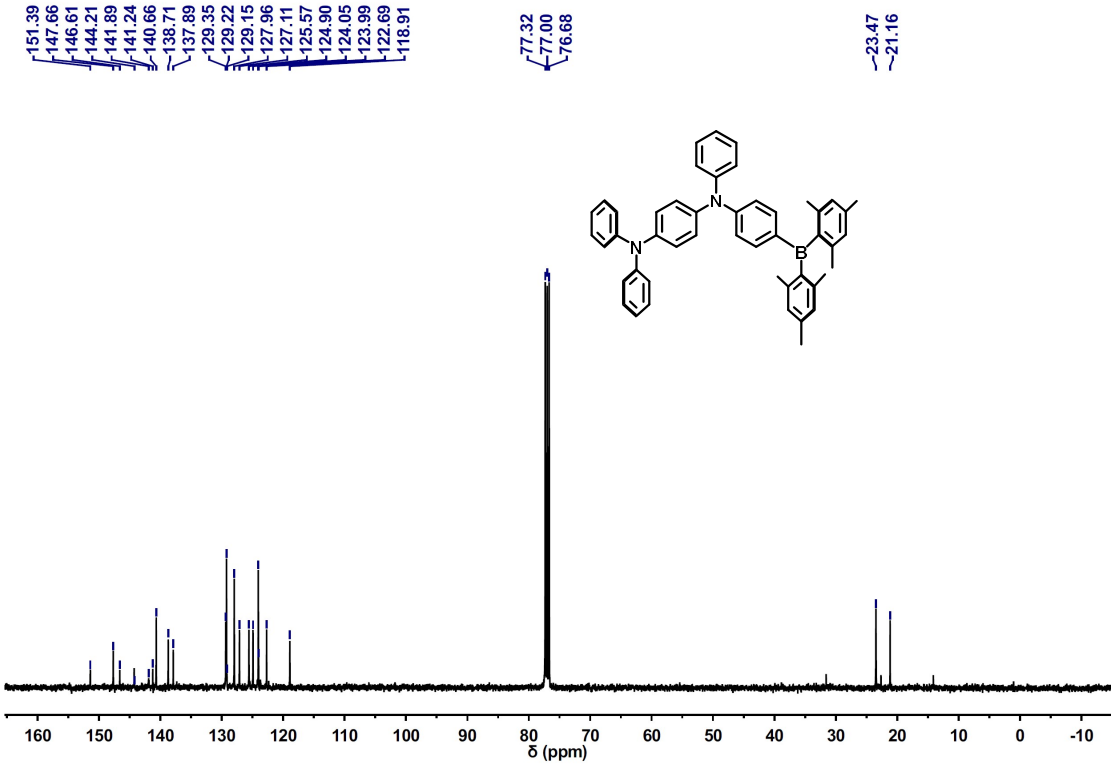

Figure S2. ^{13}C NMR spectrum of **1** in $CDCl_3$.

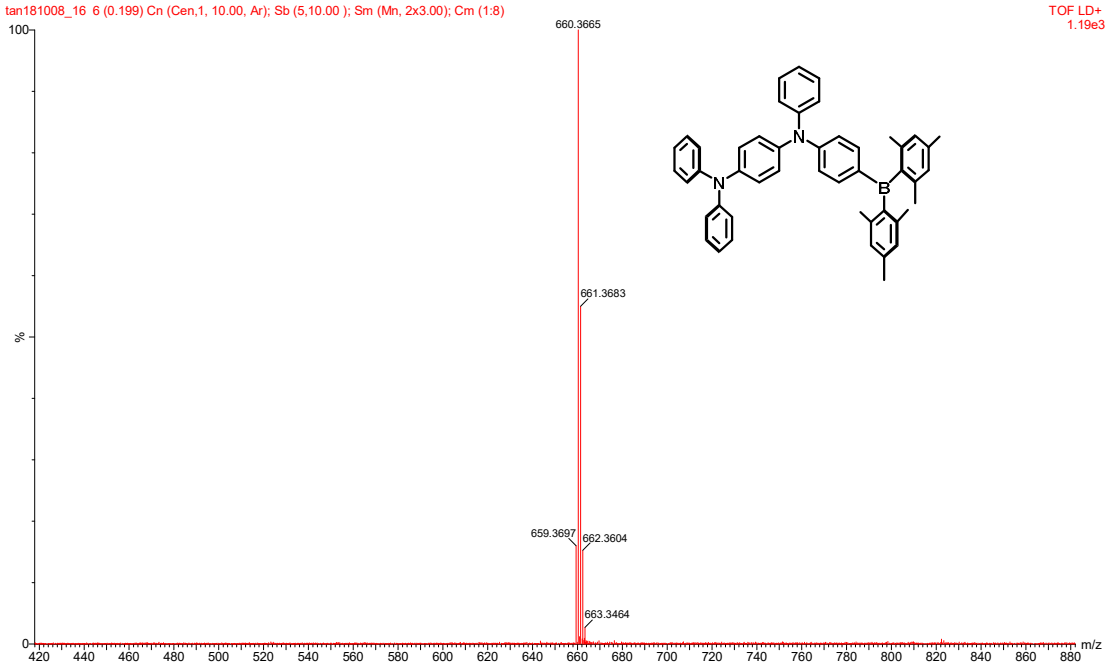

Figure S3. HR-MS spectrum of **1**.

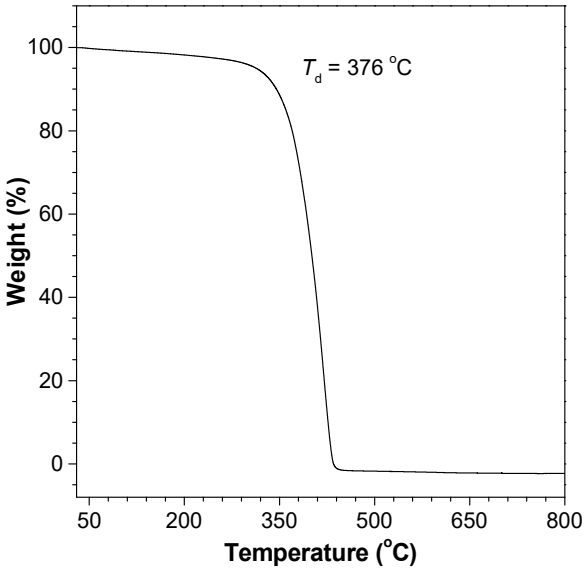

Figure S4. The TGA curve of compound **1**.

Table S1. Crystal data and parameters of data collection and refinement for compound **1**.[a)]

Compound	**1**
Empirical formula	$C_{48}H_{45}BN_2$
Formula weight	660.67
Temperature	100(2) K
Wavelength	1.54184 Å
Crystal system	Monoclinic
Space group	$P12_1/c1$
Unit cell dimensions	a = 7.5979(2) (12) Å b = 32.4387(6) Å c = 16.8075(4) Å α = 90° β = 115.761(2)° γ = 90°
Volume	3730.77(16) Å^3
Z	4
Density (calculated)	1.176 Mg/m^3
Absorption coefficient	0.507 mm^{-1}
F(000)	1408
Crystal size	0.20 × 0.20 × 0.20 mm^3
Theta range for data collection	3.687 to 67.498°
Index ranges	$-9\leq h\leq 9$, $-26\leq k\leq 40$, $-19\leq l\leq 20$
Reflections collected	21716
Independent reflections	7393 [R(int) = 0.0305]
Completeness to theta = 66.500°	99.5 %
Refinement method	Full-matrix least-squares on F^2
Data / restraints / parameters	7393 / 0 / 464
Goodness-of-fit on F^2	1.068
Final R indices [I>2sigma(I)]	$R1$ = 0.0592, $wR2$ = 0.1532
R indices (all data)	$R1$ = 0.0755, $wR2$ = 0.1638
Extinction coefficient	*n/a*
Largest diff. peak and hole	0.297 and -0.235 e.Å^{-3}

[a)] Crystallographic data for the structures reported in this work have been deposited with the Cambridge Crystallographic Data Centre as supplementary publication no. CCDC: 1884262.

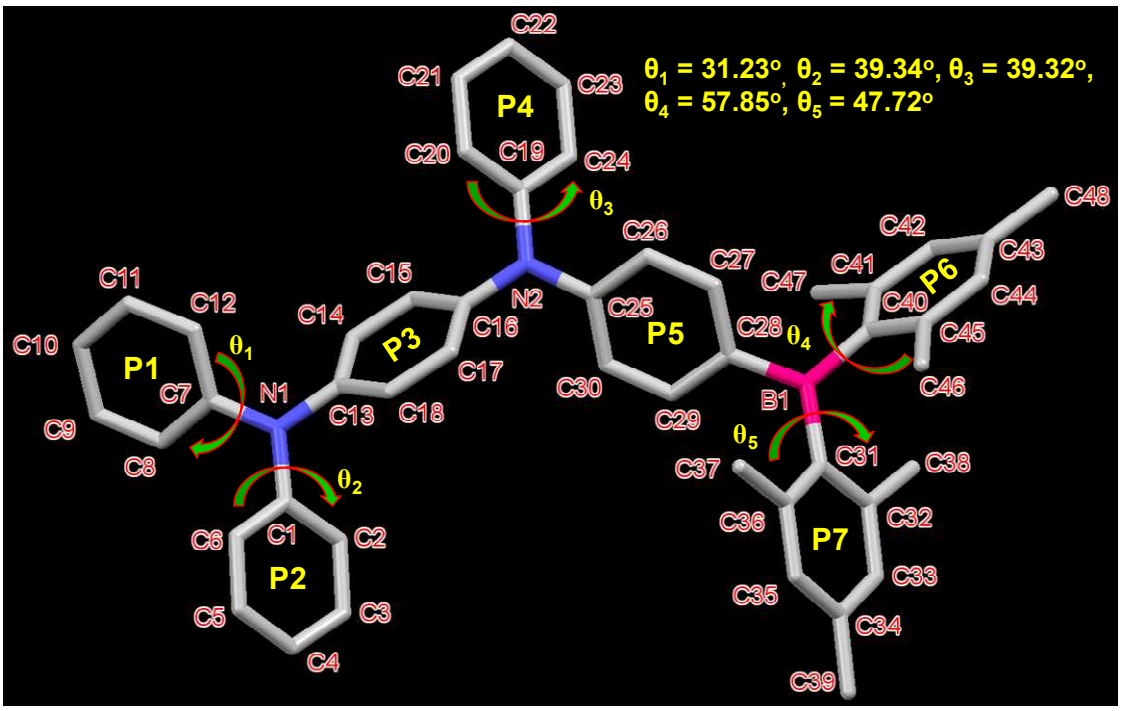

Figure S5. Crystal structure of compound **1** (P1-P7: labels of phenyl rings).

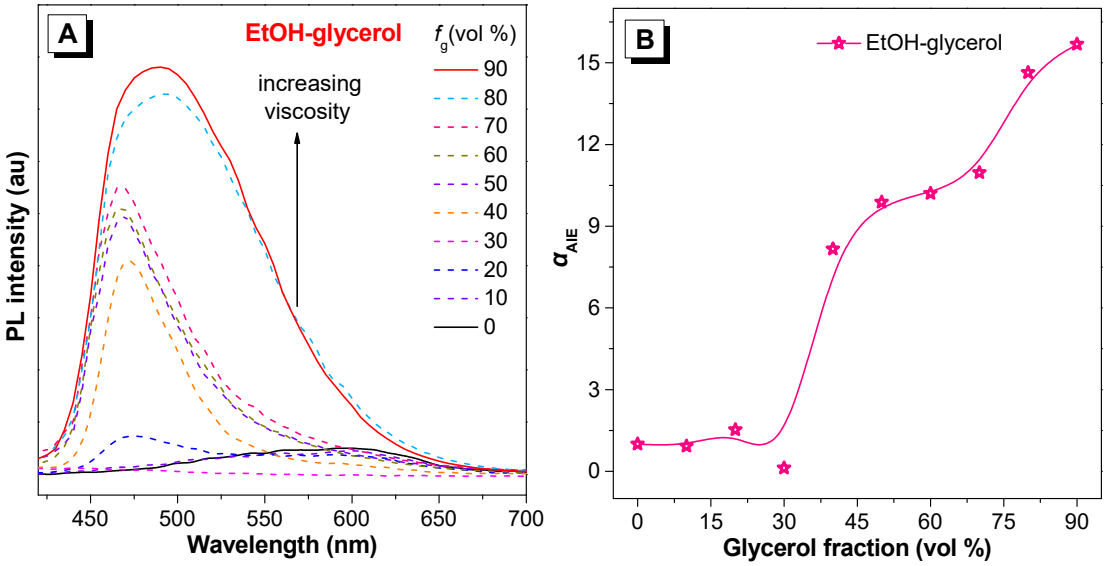

Figure S8. (A) PL spectra of compound **1** (1.0×10^{-5} M) in EtOH-glycerol mixtures, λ_{ex} = 390 nm. (B) Plot of relative maximum emission peak intensity (α_{AIE}) at 500 nm versus f_w of the EtOH/glycerol mixture, where I = emission intensity and I_0 = emission intensity in EtOH solution. Inset: Photos taken under 365 nm UV light of compound **1** in EtOH-glycerol mixtures

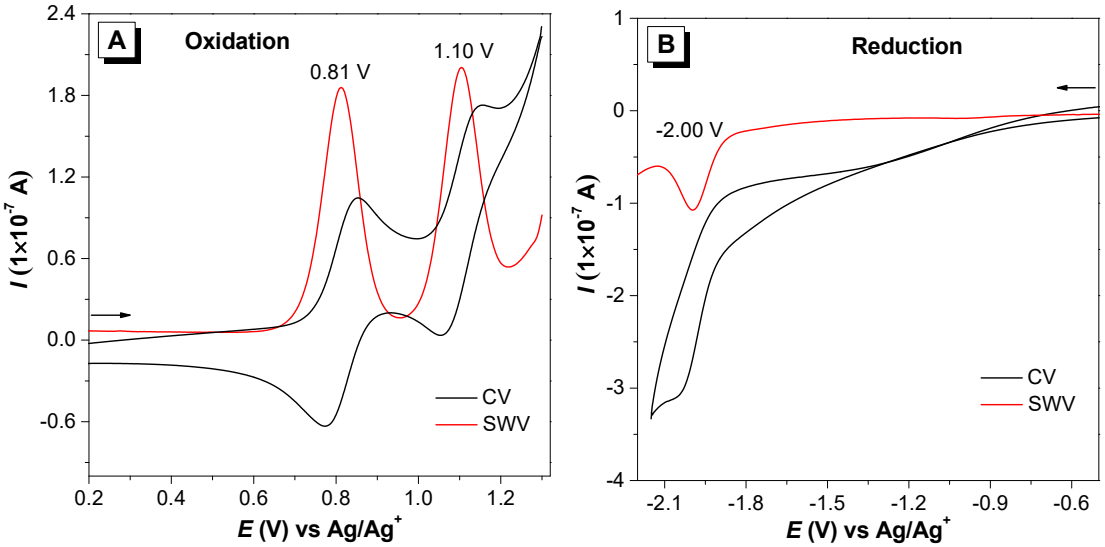

Figure S7. (A) Cyclic voltammogram (black line, THF/ 0.1 M *n*-Bu_4NPF_6, 298 K at 0.1 V s^{-1}) and (B) square-wave voltammogram curves (red line, f = 10 Hz) of compound **1**.

Table S2. Photophysical properties of compound **1** at film state.

	HOMO/LUMO[a] (eV)	T_d[b] (°C)	λ_{em}[c] (nm)	Φ_F[c] (%)	τ[c] (ns)
1	-5.18 / -2.34	376	502 nm	84	6.90

[a] The LUMO energy level was calculated from the HOMO energy level according to the equation HOMO = LUMO − E_g (HOMO = −(4.8 + E_{ox}^{onset}) eV) and E_g was calculated from the low-energy absorption onset in the absorption spectra according to the equation $E_g = 1240/\lambda_{onset}$.[6] [b] Solid state. [c] Vacuum-deposited on a quartz substrate.

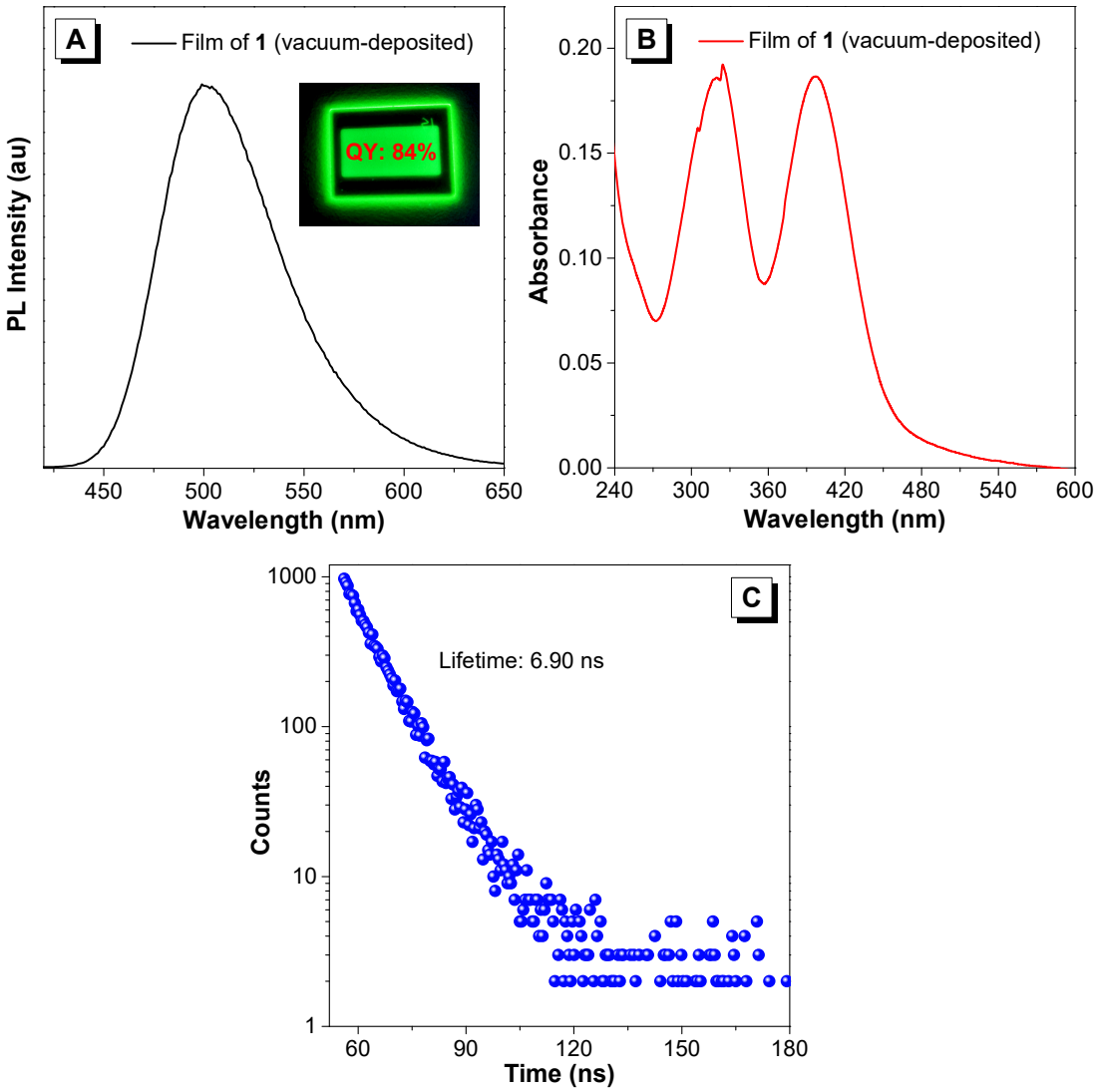

Figure S8. (A) PL and UV (B) spectra as well as PL kinetics (C) of the film for compound **1** obtained by vacuum evaporation. Inset: photo taken under 365 nm UV light and its corresponding quantum yield value.

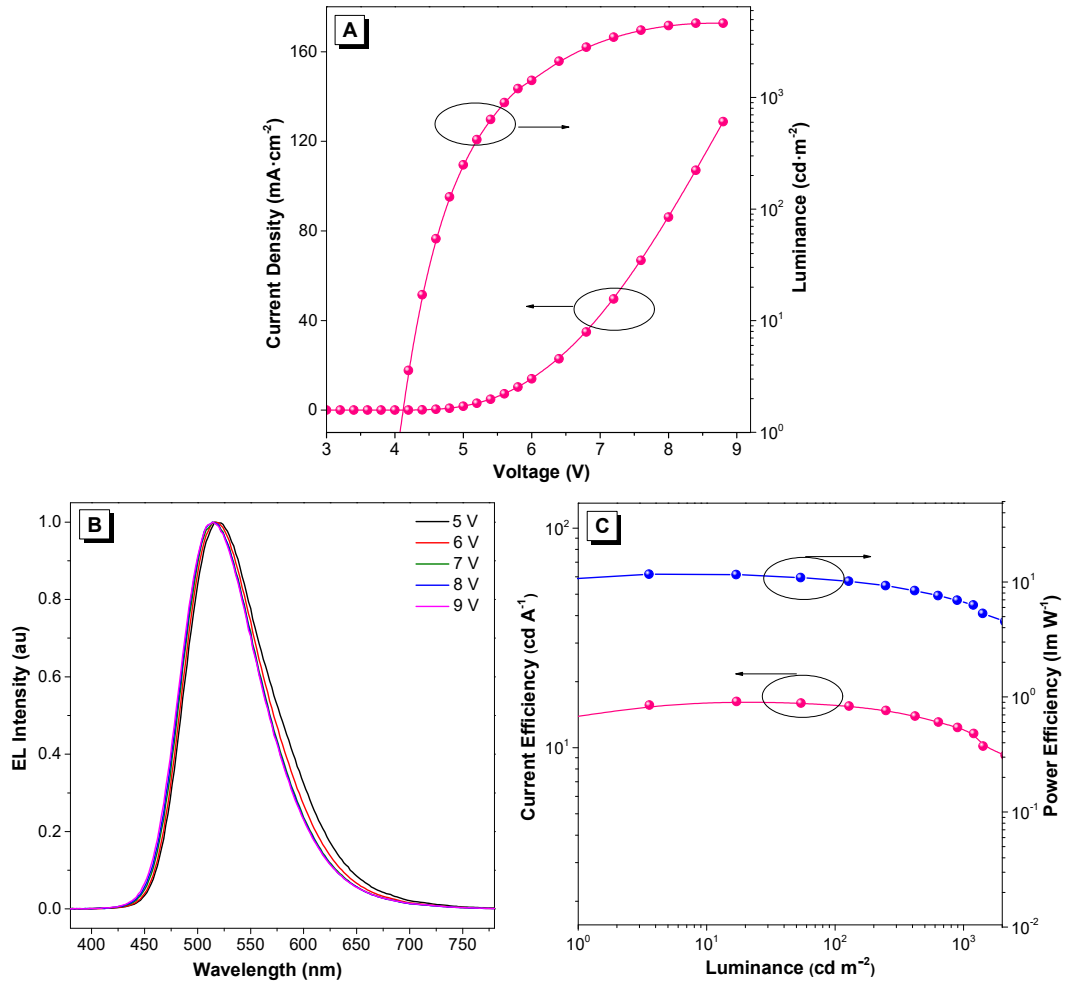

Figure S9. (A) Current density–voltage–luminance plot. (B) Voltage-dependent EL spectra and (C) CE and PE versus brightness curve of a EL device with a configuration of ITO/HATCN (5 nm)/TAPC (25 nm)/Emitter (35 nm)/TmPyPB (55 nm)/LiF (1 nm)/Al.

Table S3. EL performance of OLED.

Emitter	λ_{EL} (nm)[a]	V_{on} (V)[b]	L (cd/m^2)[a]	η_c (cd/A)[a]	η_p (lm/W)[a]	EQE (%)[a]	CIE (x, y)[c]
1	516	4.1	4622	16.23	11.69	5.22	(0.289,0.551)

[a] The luminescence (L), current efficiency (η_c), power efficiency (η_P) and external quantum efficiency (η_{ext}) are the maximum values of the device. [b] V_{on} is the turn-on voltage at 1 cd/m^2. [c] CIE coordinates at 10 mA/cm^2.

Table S4. Photophysical properties of compound **1** in different solvents.

Solvent	ν_a[a)] (nm)	ν_f[a)] (nm)	ν_a-ν_f[b)] (cm^{-1})	f[c)]	Φ[d)] (%)
Hexane	390	476	4567	0.0012	41.3
Triethylamine	390	498	5561	0.048	40.9
Isopropyl ether	390	533	6879	0.145	31.2
Ethyl ether	390	542	7191	0.167	31.7
Ethyl acetate	390	559	7752	0.2	6.7
THF	390	562	7847	0.21	8.3
DCM	390	575	8250	0.217	3.7
DMF	390	590	8692	0.276	0.8
Acetone	390	597	8891	0.284	1.1
Acetonitrile	390	608	9194	0.305	0.5

[a)] ν_a and ν_f are the UV and PL peaks in different solvents, respectively; [b)] Stokes shift in different solvents; [c)] Orientation polarization; [d)] Absolute fluorescence quantum yield.

The relationship between the Stokes shift (ν_a - ν_f) of the luminogen and solvent parameters, or the orientation polarizability $f(\varepsilon, n)$ can be described by the Lippert–Mataga equation:

$$hc(\nu_a \quad \nu_f) = hc(\nu_a^0 \quad \nu_f^0) - \frac{2(\mu_e - \mu_g)^2}{a^3} f(\varepsilon, n)$$

Where h is Plank's constant, c is the velocity of light, f is the orientational polarizability of the solvent, $\nu_a^0 - \nu_f^0$ corresponds to the Stokes shifts when f is zero, μ_e is the excited-state dipole moment, μ_g is the ground-state dipole moment, a is the solvent Onsager cavity radius, and ε and n are the solvent dielectric and the solvent refractive index, respectively.

And μ_e can be estimated according to the equation:

$$\mu_e = \mu_g + \{\frac{hca_0^3}{2} \cdot \left[\frac{d(\nu_a - \nu_f)}{df(\varepsilon, n)}\right]\}^{1/2}$$

Where the ground-state dipole, μ_g could be estimated from a long-range-correction DFT calculation based on B3LYP/6-31G(d) level, which gave a μ_g of 2.60 D. Thus, the corresponding excited-state dipole, μ_e, was calculated to be 18.6 D.

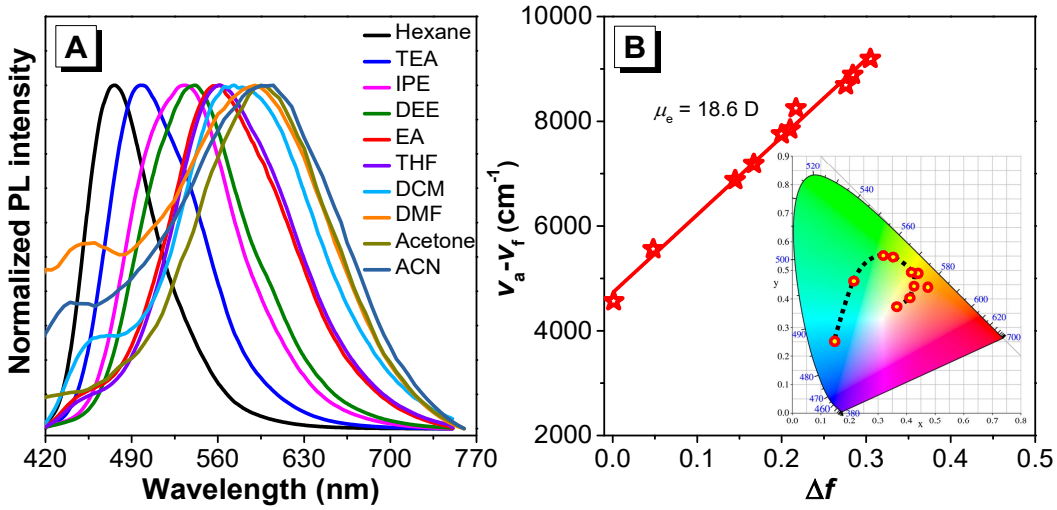

Figure S10. (A) PL spectra of compound **1** measured in different solvents. (B) Linear correlation of the orientation polarization (Δf) of solvent with Stokes shift (ν_a–ν_f) for **1** (R^2 = 0.991). Inset: CIE chromaticity diagram showing the

temperature dependence of the (x, y) color coordinates of **1**. Concentration: 1.0×10^{-5} M; λ_{ex} = 390 nm. Abbreviation: TEA = triethylamine, IPE = isopropyl ether, DEE = diethyl ether, EA = ethyl acetate, THF = tetrahydrofuran, DCM = dichloromethane, DMF = *N,N*'-dimethylformamide, ACN = acetonitrile.

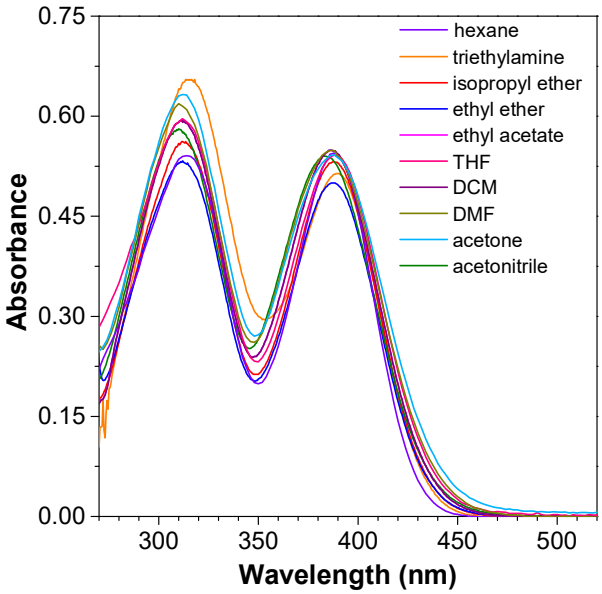

Figure S11. Absorption spectra of compound **1**, measured in different solvents with increasing polarity. Concentration: 1.0×10^{-5} M. THF = tetrahydrofuran, DCM = dichloromethane, DMF = *N,N*'-dimethylformamide.

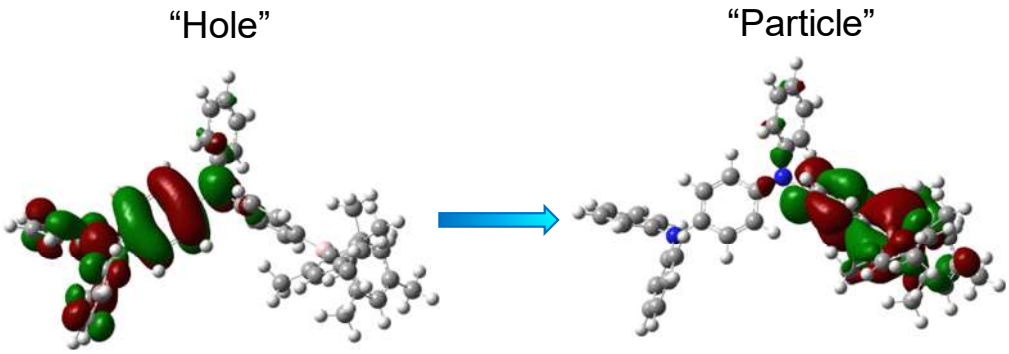

Figure S12. The natural transition orbitals (NTO) of the first singlet excited state. The contribution of the electronic transition to the first singlet excitation state is about 99%.

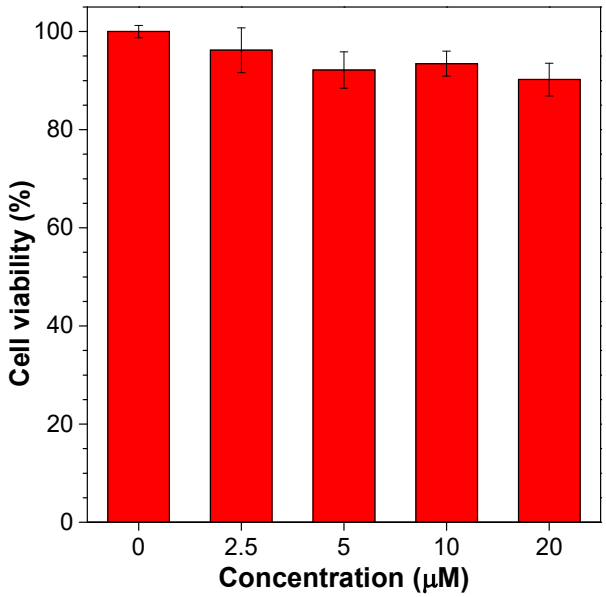

Figure S13. Cell viability of MCF-7 cells in the presence of compound **1** with different concentrations for 24 h.

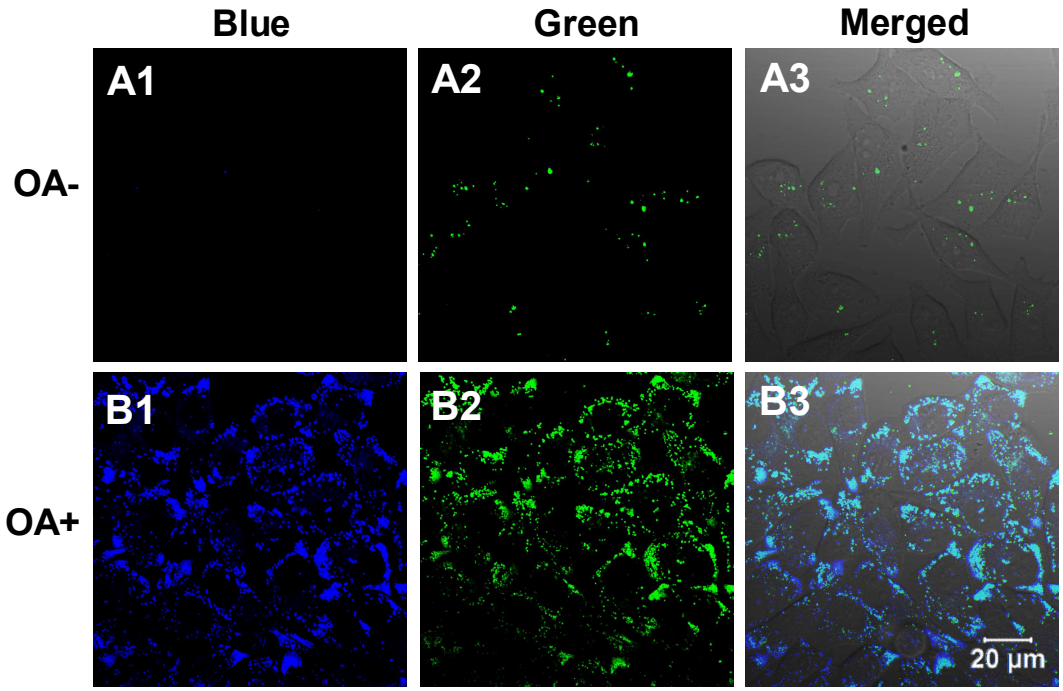

Figure S14. Two-photon microscopic images of MCF-7 cells treated with or without oleic acid (OA) and then stained with compound **1** for 1 h. Two-photon excitation wavelength: 780 nm. The two-photon fluorescence emitted from the cell were captured through two filters: 420-460 nm (blue, A1 and B1) and 495-540 nm (green, A2 and B2). A3 and B3: merged images of blue and green channels (bright field). Scale bar: 20 μm.

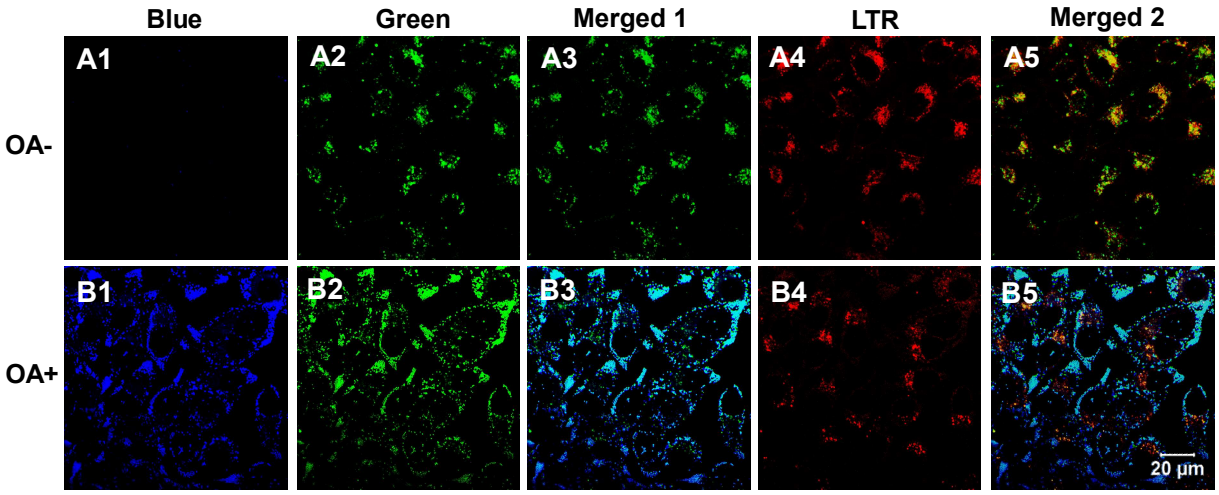

Figure S15. Two-photon microscopic images of MCF-7 cells treated with or without oleic acid (OA) and then incubated with compound **1** followed by co-staining with Lysotracker Red (LTR). Two-photon images of **1** in the emission range from λ_{em} = 420-460 nm (blue, A1 and B1), and λ_{em}=495-540 (green, A2 and B2) with excitation at 780 nm. Lysotracker Red in the emission range from λ_{em} = 575-630 nm (Red, A4 and B4) with excitation at 970 nm. Merged 1 image from panels blue and. green (A3 and B3). Merged 2 image from panels blue, green and red (A5 and B5). Scale bar: 20 µm.

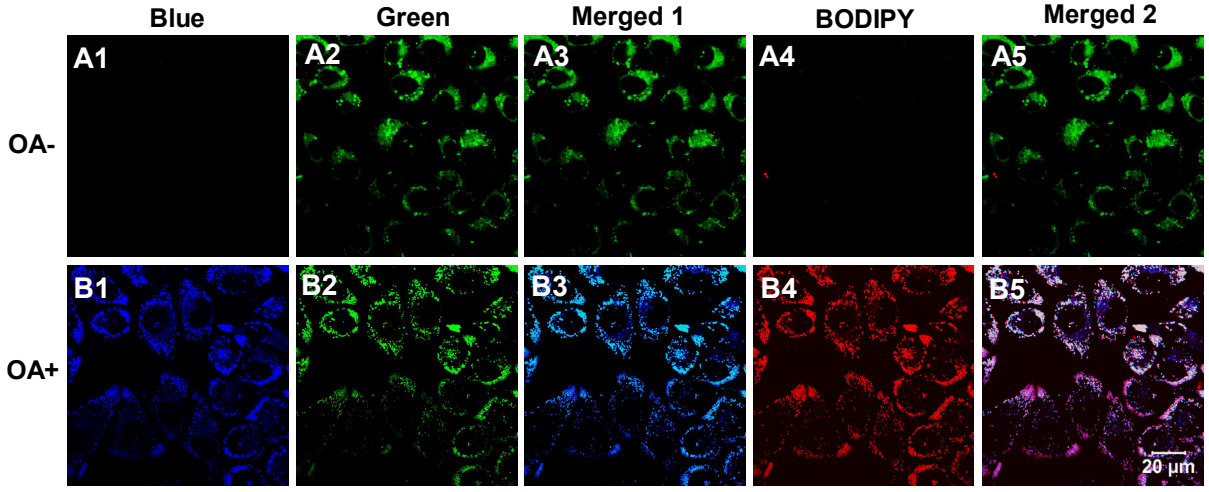

Figure S16. Two-photon microscopic images of MCF-7 cells treated with or without oleic acid (OA) and then incubated with compound **1** followed by co-staining with Lysotracker Red (LTR). Two-photon images of **1** in the emission range from λ_{em} = 420-460 nm (blue, A1 and B1), and λ_{em} = 495-540 (green, A2 and B2) with excitation at 780 nm. BODIPY in the emission range from λ_{em} = 495-540 nm (Red, A4 and B4) with excitation at 970 nm. Merged 1 image from panels blue and. green (A3 and B3). Merged 2 image from panels blue, green and red (A5 and B5). Scale bar: 20 µm.

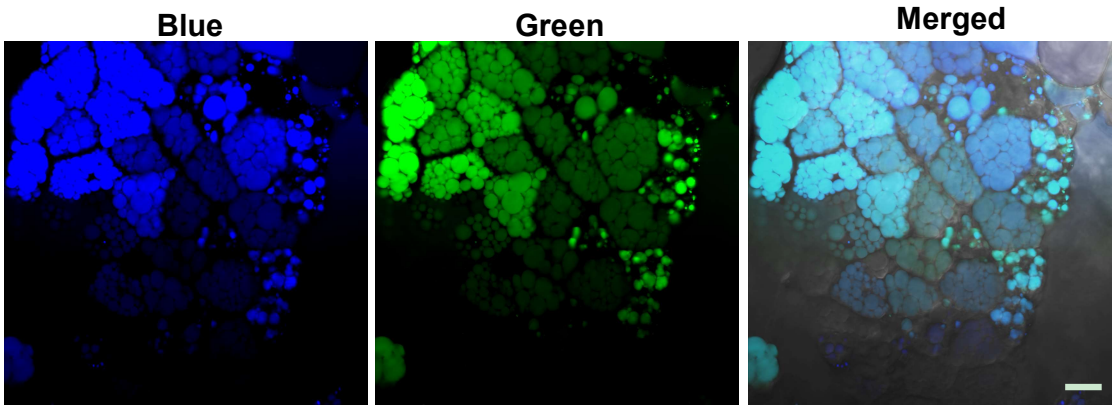

Figure S17. Two-photon microscopic images of the excised Mesenteric adipose tissues of nude mouse stained with compound **1** for 30 min. Two-photon excitation wavelength: 780 nm. Scale bar: 20 μm.

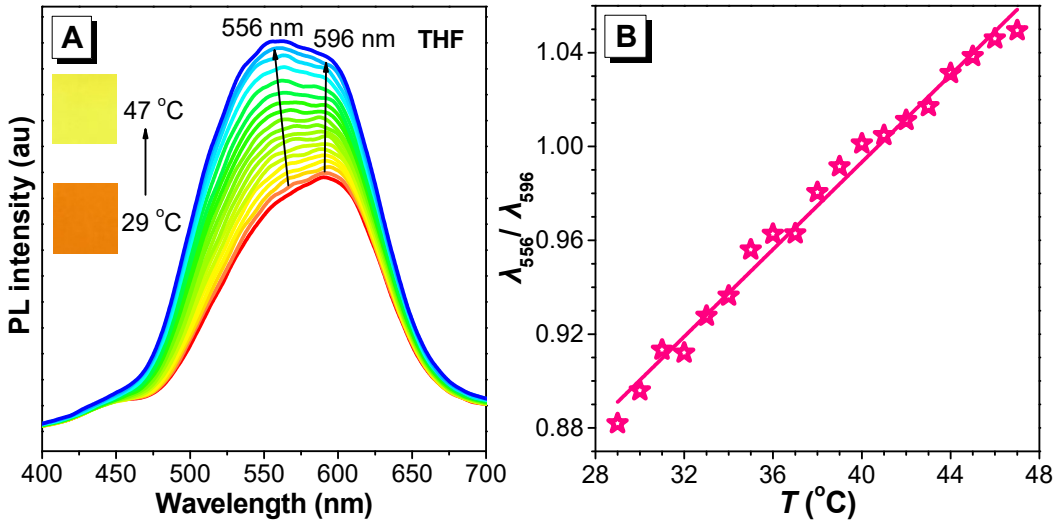

Figure S18. (A) Temperature-dependent fluorescence spectra of **1** in THF solution (1×10^{-5} M; λ_{ex} = 390 nm). (B) Plot of the corresponding intensity ratio ($\lambda_{556}/\lambda_{596}$) with temperature ($R^2$ = 0.988).

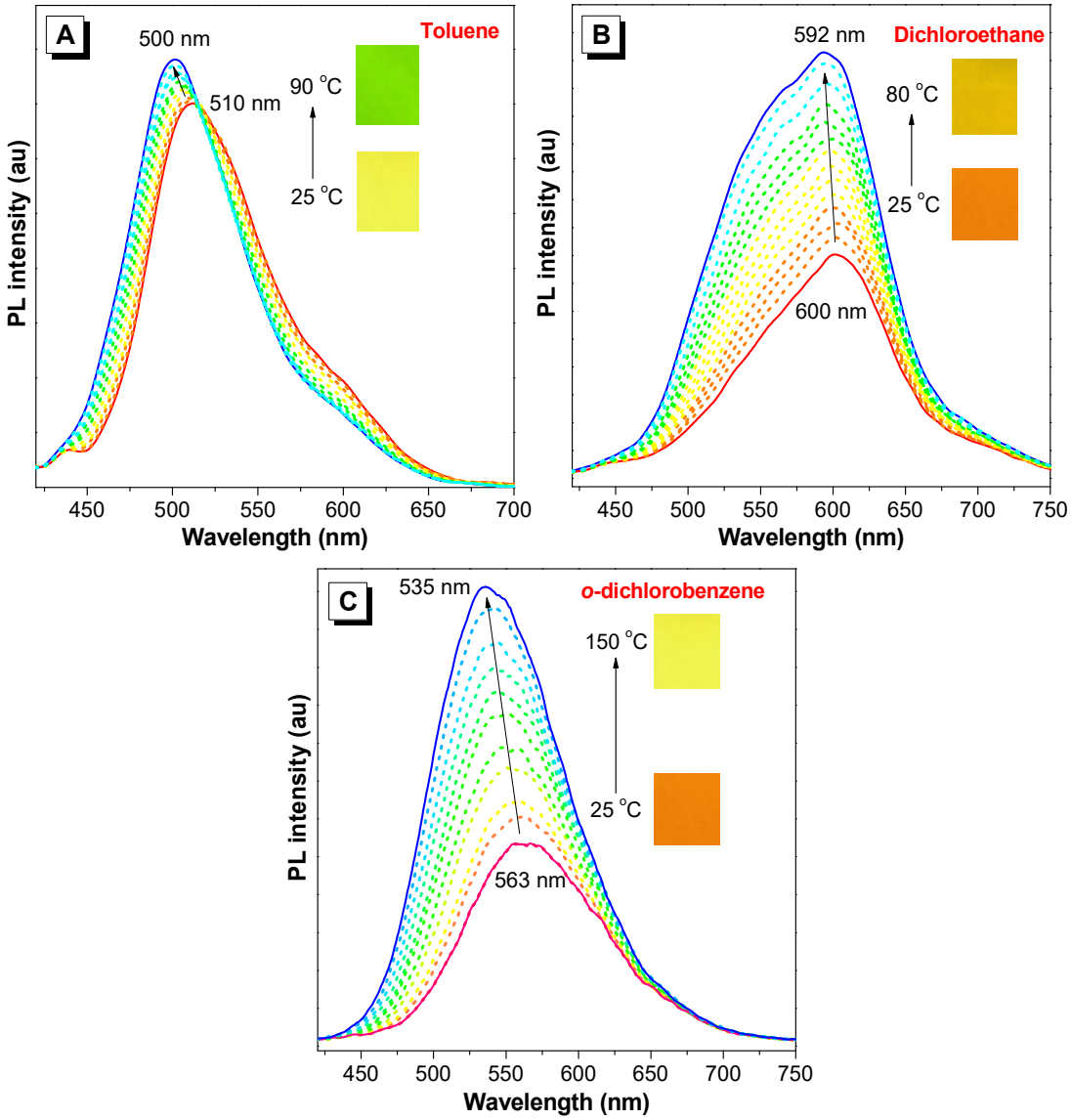

Figure S19. (A-C) Temperature-dependent fluorescence spectra of compound **1** in different solvents (1×10^{-5} M, λ_{ex} = 390 nm). Inset: Photographs of fluorescence at different temperatures.

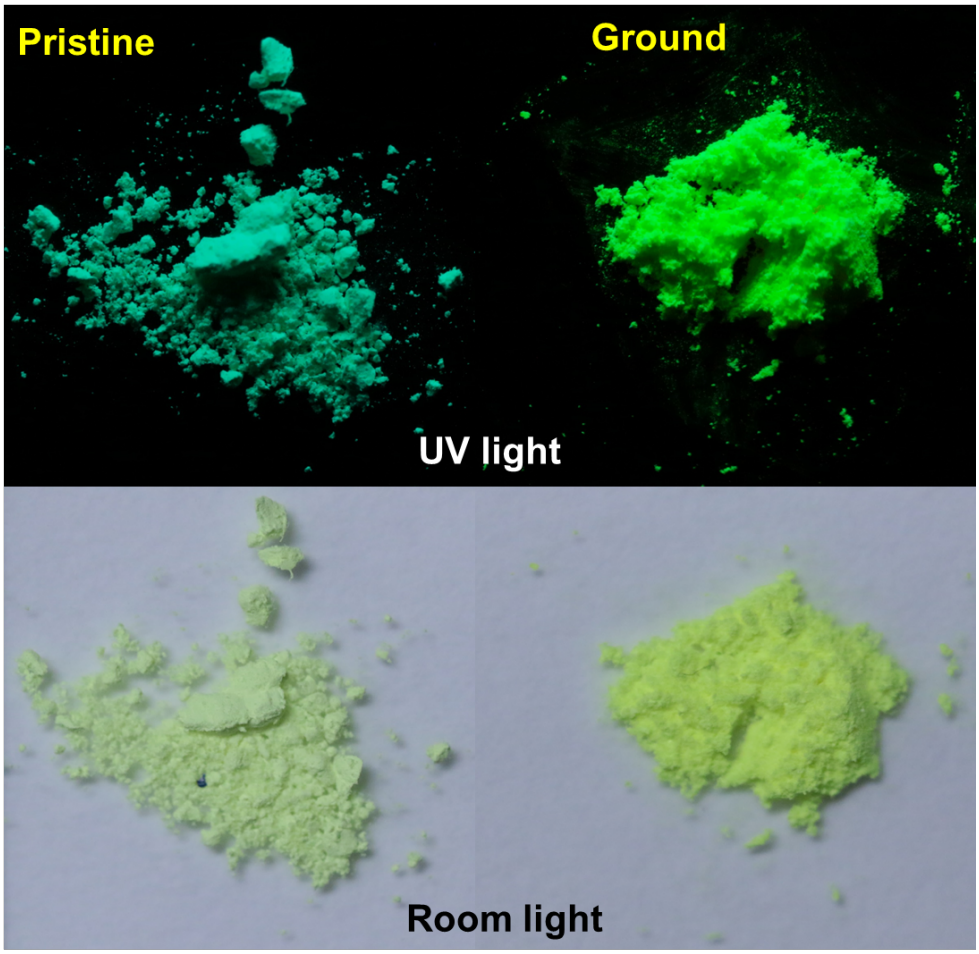

Figure S20. Photos of pristine (left) and ground (right) samples of compound **1** taken under room and UV light irradiation.

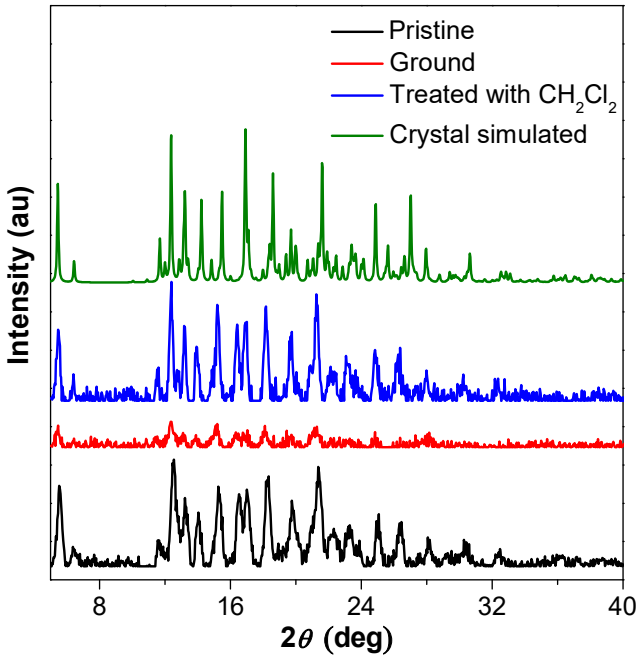

Figure S21. PXRD patterns of **1** at different states.

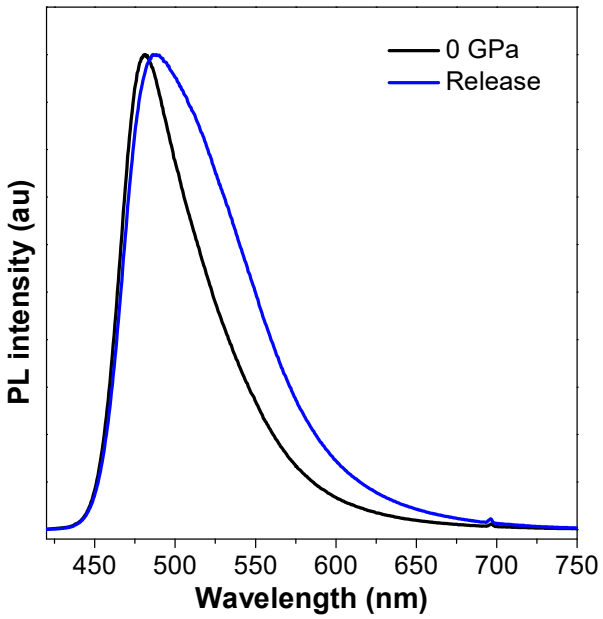

Figure S22. The recovery properties of compound **1** powder via DAC. Excitation wavelength was 365 nm.

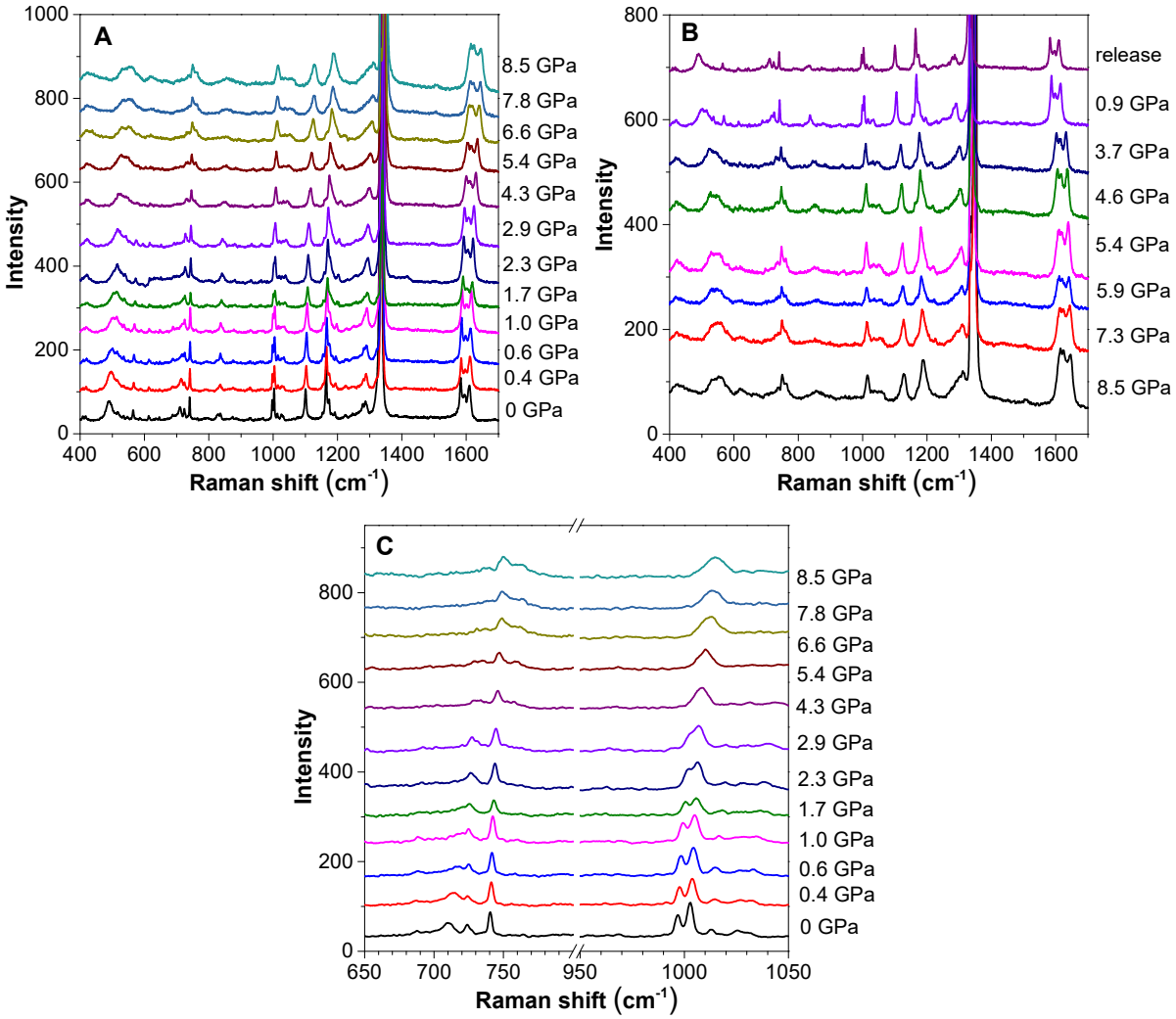

Figure S23. Raman spectra of **1** powder under different pressure values (A: compression; B: decompression; C: local presentation of A). Excitation wavelength was 365 nm.

Table S5. Experimental and DFT calculation simulated (B3LYP/6-31G(d)) Raman internal modes of compound **1**.

Experimental value (cm^{-1})	Theoretical value (cm^{-1})	Vibrational mode
709	737	C–H bond off-plane wagging vibration
723	741	C–H bond off-plane wagging vibration
740	757	C–H bond off-plane wagging vibration
997	1016	breathing vibration of benzene ring (P1, P2 and P4)
1002	1034	breathing vibration of benzene ring (P3 and P5)

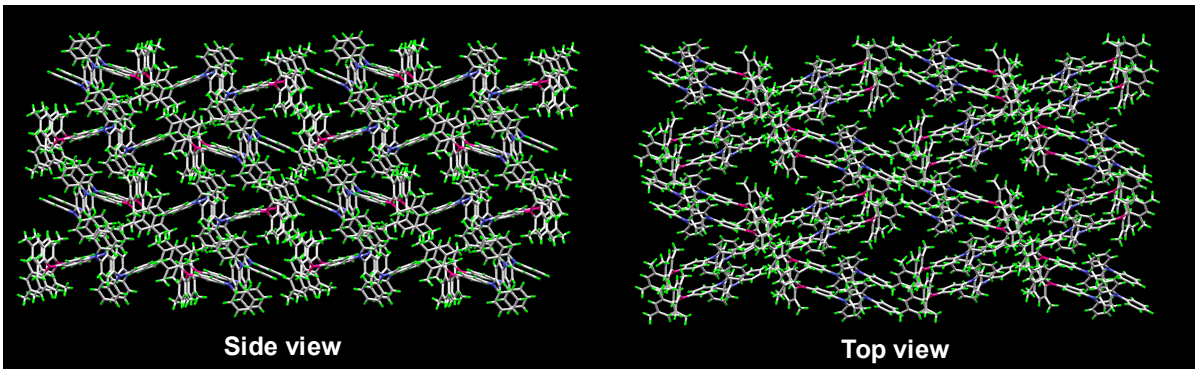

Figure S24. Molecular packings of compound **1**. Carbon, nitrogen, boron, and hydrogen atoms are shown as gray, blue, pink, and green.

References

1. G. Piermarini and S. Block, *Rev. Sci. Instrum.*, 1975, **46**, 973-979.
2. J. H. Eggert, K. A. Goettel and I. F. Silvera, *Phys. Rev. B.*, 1989, **40**, 5724.
3. H. Li, H. Wang, D. Huang, L. Liang, Y. Gu, C. Liang, S. Xu and W. Xu, *Rev. Sci. Instrum.*, 2014, **85**, 056109.
4. M. Krejčik, M. Daněk and F. Hartl, *J. Electroanal. Chem. Interfacial Electrochem.*, 1991, **317**, 179-187.
5. H.-C. Cheng, K. Y. Chiu, S. H. Lu, C.-C. Chen, Y. W. Lee, T.-F. Yang, M. Y. Kuo, P. P.-Y. Chen and Y. O. Su, *J. Phys. Chem. A*, 2015, **119**, 1933-1942.
6. C. Chi and G. Wegner, *Macromol. Rapid Commun.*, 2005, **26**, 1532-1537.